Environ. Sci. Technol. **2007**, *41,* 870−875

Potential Mobilization of Platinum-Group Elements by Siderophores in Surface Environments

SUSAN R. DAHLHEIMER, CLIVE R. NEAL,* AND JEREMY B. FEIN
Civil Engineering and Geological Sciences, University of Notre Dame, Notre Dame, Indiana 46556

The emission of platinum-group elements (PGEs) from catalytic converters has led to increased environmental abundances of Pt, Pd, and Rh; however, little is known about the environmental effects and fate of these metals. Organic ligands found in soils have the potential to increase the mobility of PGEs and potentially increase the bioavailability of the metals. Here, we assessed the abilities of microbially produced iron-chelating ligands (siderophores) to complex with the PGEs. Batch experiments using the synthetic siderophore desferrioxamine-B (DFO−B) and powdered metal or oxide forms of Pt, Pd, or Rh showed that DFO−B enhances the solubility of Pt and Pd due to the formation of Pt- and Pd−DFO−B aqueous complexes, with estimated minimum stability constants on the order of 10^{17-18} and 10^{20-24}, respectively. Dissolution rates for Pd are comparable to other mineral dissolution rates with DFO−B. DFO−B had little to no effect on the dissolution of Rh metal or Rh_2O_3. Our results indicate that siderophores have the potential to increase the mobility of Pt and Pd in environments with limited activities of free trivalent cations. These results have implications for the fate of catalytic converter-emitted Pt and Pd, and support the need for further Pt and Pd toxicity and bioaccumulation studies.

Introduction

The release of the platinum-group elements (PGEs) Pd, Pt, and Rh from catalytic converters is well documented (*1*), but little is known about PGE mobility in the environment. The submicrometer- to micrometer-sized PGE particles are emitted at ng/km rates (*1*). Due to continued and increasing emission of these metals and the adverse health affects associated with certain forms of the PGEs (*1*), the fate of PGEs in the environment warrants further study. Additionally, Pd, Pt, and Rh are precious metals, and therefore, understanding the mobility of the PGEs for potential recovery or remediation reasons is essential.

Studies considering specific routes of PGE transformation and/or transportation are limited. PGE particles have been found in river sediments still associated with the cerium support material indicating direct transport of the particles from the roadside (*1*). Plants, such as water hyacinths, cucumbers, and grass, and organisms, such as mussels, eels, and isopods, have been shown to take up and in some cases accumulate forms of the PGEs (*1*). Additionally, acidic synthetic rainwater was found to increase the solubility of Pd, Pt, and Rh (*1*). A comparison of a PGE-spiked sterile and nonsterile soil concluded that microorganisms do not increase the solubility of Pt (*2*). However, it has been demonstrated that the PGEs can be mobilized by natural organic matter (*1*). Also, humic acids, analogues for humic acid binding sites (phthalate and salicylate), and some organic ligands (e.g., L-methionone, acetate, fulvic acid) have been shown to enhance the solubility of various forms of Pt and Pd (*3*−*6*).

Siderophores represent a class of organic ligands of potential importance to the mobility of PGEs in soils. Siderophores are low molecular mass organic compounds produced by bacteria, fungi, and plants to increase the bioavailability of iron (*7*). Their concentrations in soils vary depending upon the iron content, the siderophore-producing population size, the soil horizon, and pH (*7*, *8*).

To better understand the potential transport of PGEs in the environment, we report here the results of an initial study involving the solubility of metallic and oxide forms of Pt, Pd, and Rh (as these are the dominant forms of the PGEs released by catalytic converters, refs *9*, *10*) with the synthetic siderophore desferrioxamine-B (DFO−B) (see ref *7* for chemical structure). The impetus for this study is to build an understanding of what happens to the PGEs immediately after deposition at the roadside by exploring the influence of siderophores on PGE mobility. Siderophore DFO−B is a hydroxamate-type siderophore with four binding locations that permit a high affinity for Fe(III) with a stability constant for the Fe(III)-DFO−B complex of $10^{30.7}$ (*7*). However, siderophores are also capable of complexing with other metal ions such as Al(III), Ga(III), Sn(II), and U(IV) (*11*−*13*). The high metal specificity of siderophores has led to the application of siderophore as chelators in the medical field (see ref *14*) and for potential use in nuclear fuel reprocessing and the treatment of industrial wastes (*14*).

Although the affinity of DFO−B for many metal ions is known, PGE-siderophore complexation has not been extensively studied, and the stability constants are unknown. Strong evidence from correlations between metal ion properties and metal-DFO−B stability constants suggests that PGE-DFO−B complexes could have stability constants close to that of Fe(III) or higher (*12*, *15*, *16*). Hernlem et al. (*16*). predicted a Pd−DFO−B stability constant of $10^{31.4}$, higher than that for Fe(III), from one such correlation. Additionally, brief reports of research involving $Pd(OH)_2$ and metallic forms of the PGEs indicate that siderophores do impact the solubility of PGEs albeit at a slow rate such that it may take years for equilibrium to be reached (*17*−*21*). Despite this kinetic limitation, here we compare dissolution rates and estimated minimum stability constants of the PGEs to that of other metal ions with DFO−B determined under similar conditions to the experiments reported here. This work differs from related previous work (*17*−*21*) in that we study metal oxides as well as PGE metals at a constant DFO−B concentration. From our results we evaluate the potential importance of siderophores on PGE complexation in the surface environment and the predictions made can then be tested by experiments conducted under more environmentally realistic conditions.

Experimental Section

Materials. Desferrioxamine-B (mesylate salt) as well as Pt metal, PtO_2, Pd metal, PdO, Rh metal, and Rh_2O_3 powders

* Corresponding author phone: (574)631-8328; fax: (574)631-9236; e-mail: neal.1@nd.edu.

10.1021/es0614666 CCC: $37.00
Published on Web 12/22/2006

TABLE 1. Summary of Surface Area, Particle Size Ranges, and DFO−B Dissolution Rates of the Powders[a]

sample	BET surface area (m^2/g)	approximate particle size range (μm)	dissolution rates: pH	dissolution rates: rate (nmol/m^2hr)
Pt	1.47 ± 0.04	<5	7	0.12
PtO_2	83.22 ± 0.46	15−150	7	0.02
Pd	0.24 ± 0.42	<5	7	4.26
PdO	1.19 ± 1.41	2−40	4	4.43
			7	10.14
			10	15.62
Rh	0.45 ± 0.38	2−200	7	ND
Rh_2O_3	0.46 ± 0.41	3−100	7	ND

[a] Errors for the surface area represent 2σ. Rates of DFO−B-promoted PGE dissolution (see text for details) are in the presence of 240 μMolal DFO−B. Experimental conditions were 40 μmole PGE form in 100 mL $NaClO_4$, ionic strength is 0.1. ND = value not determined

were obtained from Sigma Aldrich. Metals and metal oxides were chosen as these are the main forms of PGEs that are emitted by catalytic converters (*9*, *10*). Fortunately, PtO_2 is the reported form of emitted oxidized Pt (*22*). However, it is not clear whether oxidized Pd and Rh are in the 2+, 3+, or 4+ states. For our experiments, we chose those oxides that were commercially available. BET surface areas were determined from N_2 gas adsorption with a volumetric sorption analyzer [Coulter SA 3100 gas adsorption analyzer (Beckman Coulter, Inc., Fullerton, CA)]. Particle sizes were estimated from environmental scanning electron microscope (ESEM) images (LEO EVO-50XVP) (Table 1). Particle sizes were to be as close to the catalytic converter emissions as possible (1−30 μm, ref *1*); therefore, additional pulverization (accomplished by hand with an agate mortar and pestle) was needed for Rh_2O_3 and Rh as evidenced by the large particles in initial ESEM images. All dilutions were made with 18 MΩ−ultrapure water.

Dissolution of Metal and Metal Oxides. The siderophore−PGE interactions were monitored utilizing batch experiments at room temperature (25 °C) contained in 250-mL high-density polyethylene (HDPE) bottles (six bottles per metal form). Powder masses equivalent to 40 μmole of each PGE were added to 100 mL of 0.1 M $NaClO_4$. The unreactive electrolyte $NaClO_4$ was used to buffer the ionic strength of the solutions. All experiments were conducted at pH 7, while PdO experiments were also conducted at pH values of 4 and 10. The solution pH was measured before and throughout the experiments and was adjusted with 0.01 M and 0.1 M NaOH or 0.01 M HCl (the latter only used for pH 4 PdO experiments). The pH was not buffered, and therefore, pH values ranged from 3.98 to 4.17, 6.60 to 7.21, and 9.60 to 9.96 throughout the experiments. The bottles were placed on a shaker table (128 lateral movements/min). After the "time zero" initial sample, DFO−B was added to three bottles in each set (the other three bottles served as controls) for a siderophore concentration of 240 μMolal. This concentration is at the lower end of the range of siderophore concentrations estimated to be in a soil based on bacterial siderophore production (*23*) and allows the results to be more widely compared with other siderophore-metal complexation studies (*23*−*26*).

Before sampling, the bottles were centrifuged at 6000 rpm for 10 min. Samples (3.5 mL) were then drawn from the solution and filtered (0.45 μm filters Cameo Nylon) into 12-mL Teflon beakers to ensure no particles were in the samples. The solution removed was replaced with stock solutions of either 0.1 M $NaClO_4$ for the controls or 240 μMolal DFO−B in 0.1 M $NaClO_4$. This procedure results in a slight dilution of the metals over time, but is minimal relative to the increase in the liquid: solid ratio that would have occurred without such additions. All pHs were recorded and adjusted back to the desired pH after sampling.

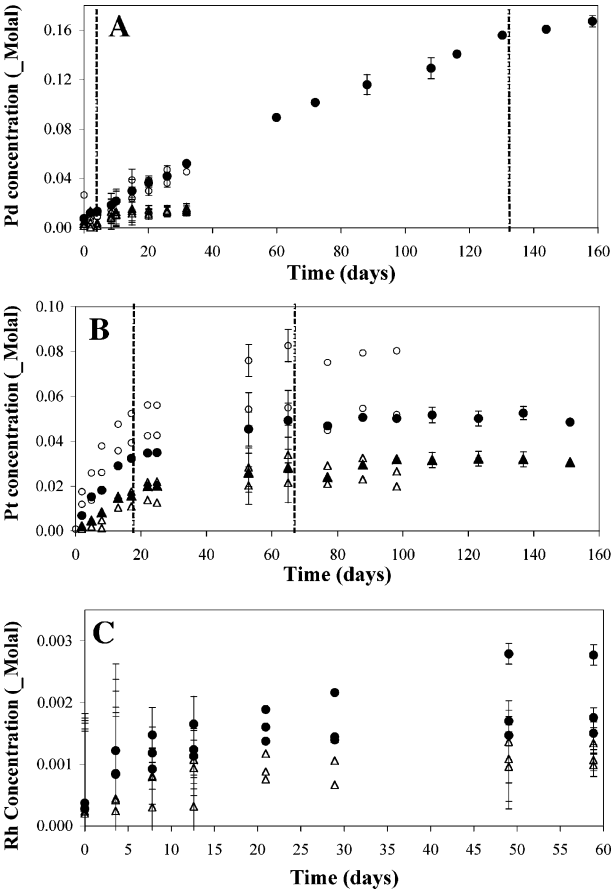

FIGURE 1. Batch dissolution results for metallic Pd (A), Pt (B), and Rh (C). Controls with no DFO−B (triangles) are shown. Experiments with DFO−B (circles) contained 240 μMolal DFO−B. Error bars represent 95% confidence intervals of the regression analysis (calculated after the method of ref *38*) and are omitted if they do not exceed the size of the symbol. Unfilled data points distinguish the replicates that were removed from the experiment (see text for details). The vertical dotted lines indicate the separation of the fast initial dissolution, constant dissolution rates, and steady-state dissolution. Experimental conditions were 40 μmole PGE form in 100 mL $NaClO_4$, ionic strength is 0.1, pH is 7.

Sample Preparation and Analysis. Samples were prepared and analyzed according to procedures described in the Supporting Information. Analyses were performed using the high-resolution Thermo Finnigan element 2 inductively coupled plasma mass spectrometer (ICP−MS). The average detection limits (3 σ) determined from blanks were 0.4 nMolal (42.5 pg/g), 0.02 nMolal (3.96 pg/g), and 0.002 nMolal (0.21 pg/g) for Pd, Pt, and Rh, respectively.

Results and Discussion

Extent of Dissolution. Dissolution of metallic Pd, Pt, and Rh at pH 7 was monitored over time (Figure 1). Due to the length of the experiments and shaker table space limitations, after a clear separation between the three controls and the three bottles containing siderophore became evident, five bottles were removed and one bottle containing siderophore was left for further reaction. In the case of Pt metal, one control also was left. After 25 days, the Pd concentration in solution with DFO−B was over 2.5 times higher than in the absence of DFO−B (Figure 1A). Platinum metal was less affected by the presence of DFO−B with an aqueous Pt concentration only 1.5 times greater than the inorganic control after 25 days (Figure 1B). The Rh experiment, although not monitored

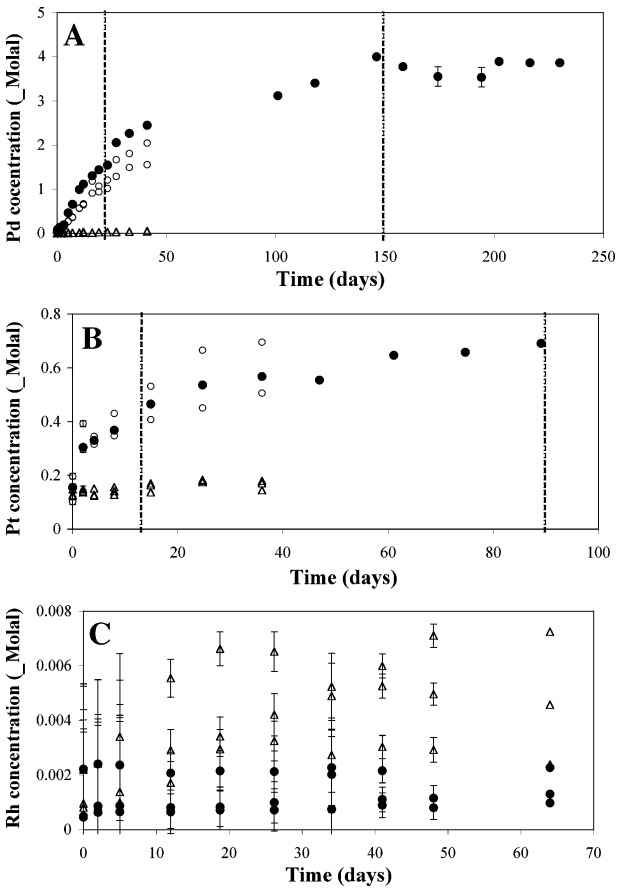

FIGURE 2. Batch dissolution results for PdO (A), PtO_2 (B), and Rh_2O_3 (C). Controls with no DFO−B (triangles) are shown. Experiments with DFO−B (circles) contained 240 μMolal DFO−B. Error bars represent 95% confidence intervals of the regression analysis (calculated after the method of ref *38*) and are omitted if they do not exceed the size of the symbol. Unfilled data points distinguish the replicates that were removed from the experiment (see text for details) The vertical dotted lines indicate the separation of the fast initial dissolution, constant dissolution rates, and steady-state dissolution. Experimental conditions were 40 μmole PGE form in 100 mL $NaClO_4$, ionic strength is 0.1, pH is 7.

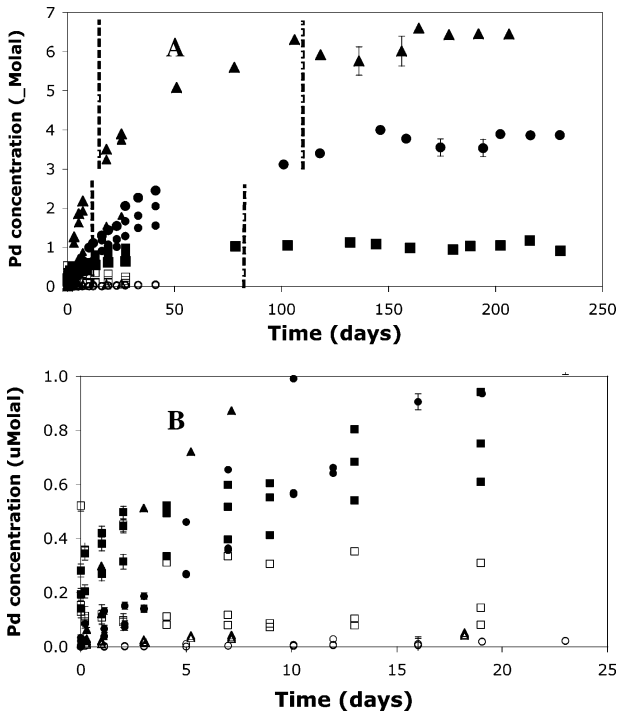

FIGURE 3. Batch dissolution data for the PdO at pH 4 (squares), 7 (circles), and 10 (triangles). B depicts detail of short time/low concentration region of A. Controls (no DFO−B), represented by unfilled symbols, are shown. Experiments with DFO−B (filled symbols) contained 240 μMolal DFO−B. The vertical dotted lines indicate the separation of the fast initial dissolution, constant dissolution rates, and steady-state dissolution for pH 4 and 10 conditions. Error bars represent 95% confidence intervals of the regression analysis (calculated after the method of ref *38*) and are omitted if they do not exceed the size of the symbol. Experimental conditions were 40 μmole Pd in 100 mL $NaClO_4$, ionic strength is 0.1.

for as long as Pt or Pd, showed much less dissolution both with and without DFO−B (Figure 1C); however, after 60 days, we observed a slight enhancement of dissolution due to DFO−B in only one of the experiments.

The dissolution of the PGE-oxides was more extensive than the metallic PGEs (Figure 2). After approximately 25 days, we measured 42 times the concentration of Pd and only 2.5 times the concentration of Pt in the solutions containing DFO−B compared to their respective concentrations in the inorganic controls (Figure 2A and 2B). The degree of dissolution of Rh_2O_3 was 2−3 orders of magnitude less than the other PGE oxides. For Rh_2O_3, DFO−B appeared to inhibit dissolution (Figure 2C). Overall, the results of the Rh and Rh_2O_3 experiments (Figures 1C and 2C) were unexpected, as Rh(III) has ion properties most similar to Fe(III).

The results presented here are strong evidence that Pd- and Pt−DFO−B aqueous complexes formed under the experimental conditions. Additionally, PdO experiments conducted at pH values of 4, 7, and 10 showed that the formation of these complexes likely increases with pH, as at high pH more metal was solubilized (Figure 3). The proton-active sites of DFO−B exhibit negative log acidity constants (pKa) of 10.87, 9.57, 8.97, and 8.35 (ionic strength = 0.1, T = 25 °C) (*12*). Therefore, at pH 10, only the amine group (with a pKa of 10.87) is protonated, and Pd(II) is able to bind at deprotonated sites. Thus, the pH 10 experiment resulted in the greatest Pd concentration in solution. Our experiments provided evidence of Pd complexation at pH 7 and pH 4 also, where DFO−B is fully protonated, suggesting that the bonding is more than electrostatic ion-pairing and that a significant degree of inner-sphere or covalent bonding occurs.

Dissolution Rates. The results not only demonstrate the formation of aqueous PGE−DFO−B complexes, which enhance the extent of dissolution, but we also observed enhanced dissolution rates in the presence of DFO−B, likely due to the destabilization associated with the presence of surface PGE−DFO−B complexes. The PGE concentrations in solution reached steady state for PdO (pH 4, 7, and 10) and metallic Pt. For these experiments, we observed three dissolution stages: initial rapid dissolution, a slow dissolution with a relatively constant dissolution rate, and steady-state dissolution. For comparison, we calculated the rates of dissolution normalized to the surface area for the PdO, PtO_2, Pd, and Pt (Table 1) experiments based on the following equation:

$$R = \frac{1}{A \cdot m} \cdot \frac{d[M]_{\text{diss}}}{dt} \quad (1)$$

where R is the dissolution rate (nmol·m^{-2}·hr^{-1}), A is the surface area (m^2·g^{-1}) (reported in Table 1, and is assumed to remain constant throughout the experiments), m is the solids concentration (g· L^{-1}), $[M]_{\text{diss}}$ is the dissolved metal concentration (nmol·L^{-1}), and t is time (hr) (*27*). We used the second stage of dissolution in each experiment (shown in Figures 1−3) to compute $d[M]_{\text{diss}}/dt$. We identified the

TABLE 2. Chemical Reactions with Their Corresponding Equilibrium Constants and Equations Used to Model the Pd and Pt Experiments for the Determination of the Pd/Pt−DFO−B Stability Constants (K_f) from the Experimental Data Reported Here[a]

		Log *K*	source	modeled Log *K*
(T1)	$Pt(s) + 2H+ + 0.5O2 \leftrightarrow Pt2+ + H_2O$	−0.2	*29*	
(T2)	$Pt2+ + OH- \leftrightarrow Pt(OH)^+$	24.91	*33*	14.16
(T3)	$Pt^{2+} + 2OH^- \leftrightarrow Pt(OH)_2$	28.81	*33*	21.34
(T4)	$PtO_2(s) + 2H^+ \leftrightarrow Pt^{2+} + H_2O + 0.5O_2$	13.28[b]	*39*	0.39, 0.63[c]
(T5)	$Pd(s) + 2H^+ + 0.5O_2 \leftrightarrow Pd^{2+} + H_2O$	10.6	*29*	−3.23
(T6)	$Pd^{2+} + OH^- \leftrightarrow Pd(OH)^+$	12.58*	*35*	
(T7)	$Pd^{2+} + 2OH^- \leftrightarrow Pd(OH)_2$	24.15*	*35*	
(T8)	$Pd^{2+} + 3OH^- \leftrightarrow Pd(OH)_3^-$	27.29*	*35*	
(T9)	$PdO(s) + 2H^+ \leftrightarrow Pd^{2+} + H_2O$	0.11[a]	*36*	−2.64, −3.15, −3.01[d]
(T10)	$Pd^{2+} + Cl^- \leftrightarrow PdCl^+$	5.23	*37*	
(T11)	$Pd^{2+} + 2Cl^- \leftrightarrow PdCl_2$	8.86	*37*	
(T12)	$Pd^{2+} + 3Cl^- \leftrightarrow PdCl_3^-$	11.36	*37*	
(T13)	$Pd^{2+} + 4Cl^- \leftrightarrow PdCl_4^{2-}$	12.33	*37*	
(T14)	$Pd^{2+} + 3Cl^- + OH^- \leftrightarrow PdCl_3(OH)^{2-}$	20.29	*35*	
(T15)	$H^+ + DFOB^{3-} \leftrightarrow HDFOB^{2-}$	11.49*	*12*	
(T16)	$H^+ + HDFOB^{2-} \leftrightarrow H_2DFOB^-$	9.98*	*12*	
(T17)	$H^+ + H_2DFOB^- \leftrightarrow H_3DFOB$	9.17*	*12*	
(T18)	$H^+ + H_3DFOB \leftrightarrow H_4DFOB^+$	8.35*	*12*	
(T19)	$H_2O \leftrightarrow H^+ + OH^-$	−14		
(T20)	$\sum Pd(aq)_{TOTAL} = Pd^{2+} + Pd(OH)^+ + Pd(OH)_2 + Pd(OH)_3^- +$ PdHDFOB + (all PdCl species for PdO pH 4)			
(T21)	$\sum Pt(aq)_{TOTAL} = Pt^{2+} + Pt(OH)^+ + Pt(OH)_2 +$ PtHDFOB			
(T22)	$\sum DFOB_{TOTAL} = DFOB^{3-} + HDFOB^{2-} + H_2DFOB^- + H_3DFOB + H_4DFOB^+ +$ H(Pt/Pd)DFOB			
(T23)	$\sum Cl^-_{TOTAL} = PdCl^+ + Cl^- + 2 \times PdCl_2 + 3 \times PdCl_3 + 4 \times PdCl_4^{2-} + 3 \times PdCl_3(OH)^{2-}$			

[a] * Indicates values reported for pH 4, 7, and 10, respectively; NA indicates data are not available. [b] Value was calculated from data in the specified source. [c] Values determined using modeled log K(2) or K(3), respectively; [d] Indicates value was corrected to ionic strength = 0 using the extended Debye−Hückel formula.

second stage of dissolution to include the data points that result in the best regression analysis (R^2 value closest to 1).

These surface-area normalized dissolution rates are comparable to other DFO−B-enhanced dissolution rates determined in a similar manner. For example, the highest dissolution rate we observed was 15.62 nmol·m^{-2}·hr^{-1} for PdO at pH 10 (Table 1). This rate is similar to the dissolution rate of UO_2 in the presence of DFO−B (30 nmol·m^{-2}·hr^{-1} with 200 μM DFO−B) (*11*). The dissolution rates of Pd and PdO were greater than the dissolution rates determined for goethite of 0.57 nmol·m^{-2}·hr^{-1} with 240 μM DFO−B (*28*).

Modeling. The objective of the thermodynamic modeling was to place constraints on the magnitude of the stability constants (K_f) for the PGE−DFO−B aqueous complexes that affect mineral dissolution in the experiments. By comparing these calculated stability constants to stability constant values for other metal-DFO−B complexes, we can estimate the importance of DFO−B in enhancing PGE mobilities in the environment. We assumed that the aqueous complexation reactions have the following 1:1 stoichiometry as other transition metal-DFO−B complexes (*16*):

$$M^{2+} + HDFOB^{2-} \leftrightarrow MHDFOB^0,$$

$$\text{with } K_{f(M)} = \frac{a_{MHDFOB^0}}{a_{M^{2+}} \cdot a_{HDFOB^{2-}}} \quad (2)$$

where M represents the PGE of interest (either Pd or Pt) and *a* represents the activity of the indicated species. Although the experimental data did not rigorously demonstrate the attainment of equilibrium through reversal experiments, we did observe a steady state for PdO (pH 4, 7, 10) and Pt metal (pH 7) experiments for the systems containing DFO−B. For this paper, we interpret these steady-state values as likely representing minimum concentrations of dissolved PGE in equilibrium with each solid of interest, our calculations place constraints on the minimum value of K_f.

The reactions listed in Table 2 are the important reactions that occur in the experimental systems. As Pt(II) is the predominant species across a wide range of oxygen fugacity and pH at 25 °C (*29*), the Pt(IV) species was omitted from this work. Also Wood et al. (*30*). showed that formation of $Pt(OH)_3^-$ and $Pt(OH)_4^{2-}$ occurs only at high pH; therefore, these species were omitted. Mass-action equations for appropriate reactions (Table 2), along with mass-balance constraints on the total concentration of PGE metal of interest, DFO−B, and chloride provided a complete description of the activities of each species in the experimental solutions. Knowing the *K* values for each reaction, and knowing or measuring $\Sigma PGE(aq)_{TOTAL}$, $\Sigma DFOB_{TOTAL}$, ΣCl^-_{TOTAL}, and H^+ for each solubility measurement and assuming O_2 is in equilibrium with the atmosphere, we then used a Newton−Raphson iteration approach (e.g., ref *31*) to compute the unknown stability constant values. We used the extended Debye−Hückel equation (*32*) to account for varying ionic strengths with å = 5.50 for $NaClO_4$.

Stability constant calculations for aqueous PGE-DFO−B complexes are based on the degree of solubility enhancement that we observed relative to that of the DFO−B-free systems. Unfortunately, the equilibrium constants that define the chemical speciation in the inorganic PGE systems are not well-constrained (e.g., for reactions T2, or T3, and T4, refs *33*, *34*, *39*). In our approach to modeling the Pt metal system, we assumed that the equilibrium constant for reaction T1 [K(T1)] is correct, and we calculated an equilibrium constant for reactions T2 or T3 using the measurements of Pt metal solubility in the absence of DFO−B. These calculated values are listed in Table 2 as "Modeled Log *K*" values. For the PtO_2 experiments, we calculated the equilibrium constant for

reaction T4 using the Gibbs free energies of formation of Pt^{2+} and PtO_2 compiled by Brookings (*39*). However, the calculated equilibrium constant for reaction T4 yields a predicted PtO_2 solubility under our experimental conditions that is orders of magnitude higher than what was measured. Because the calculated equilibrium constant is inconsistent with our experimental observations, we used our calculated values for K(T2) or K(T3) to determine calculated values for K(T4) based on the measured PtO_2 solubility in the absence of DFO−B, and these calculated values are also listed in Table 2. Chloride reactions (reactions T10−T14) were incorporated only in the model for PdO dissolution where pH 4, as this was the only experiment that included a pH adjustment using HCl.

The inorganic reactions, along with the reactions involving the DFO−B species, were used to quantify the minimum stability constants for the Pd- and Pt−DFO−B complexes (reaction 2), again with the assumption of 1:1 stoichiometry. Considering the data points in the steady-state stage of the Pt metal dissolution experiments, and using either K(T2) or K(T3), resulted in a log $K_f = 16.9 \pm 0.3$ or 17.2 ± 0.2, respectively (2σ uncertainties reported). Using the highest measurement of PtO_2 solubility in the presence of DFO−B, and applying values for either K(T2) or K(T3) and our calculated value for K(T4), we calculated values for log K_f of 18.2 or 18.05, respectively. The Pt metal and PtO_2 experiments yielded similar values for the estimated minimum Pt(II)−DFO−B stability constants of approximately 10^{17}−10^{18}.

We applied a similar approach to determine the Pd−DFO−B stability constant; however, in this case, values of K(T6)−K(T8) are better constrained and we used these values without adjustment. We used the Pd metal inorganic solubility measurements to calculate a value for K(T5), and we applied this value to model the DFO−B-bearing Pd metal system with the data from the last sampling to obtain a log $K_f = 20.05$ for the Pd−DFO−B complex. Applying the same approach to the PdO experiments at pH 4, 7, and 10 yielded log K_f values of 23.6 ± 0.9, 22.2 ± 0.1, and 21.9 ± 0.3, respectively, using the Pd concentrations and pH values for the data points in the steady-state stage of dissolution. The log K_f values determined from the PdO and the Pd metal solubility experiments are in reasonable agreement, given the uncertainties associated with the equilibrium constants for the inorganic reactions, and the estimated minimum stability constant for the Pd(II)−DFO−B complex is between 10^{20} and 10^{24}.

The estimated minimum PGE−DFO−B stability constants are highly dependent on the equilibrium constants used in the modeling; however, the approach used here minimizes the effects of these uncertainties. Interestingly, the minimum stability constant of Pt(II)−DFO−B is smaller that that for Pd(II)−DFO−B, which is the opposite of that seen for Pd(II) and Pt(II) complexation with inorganic ligands (*29*). Also, the measured minimum stability constants are lower than the estimated ones reported in the literature (e.g., 29, 33−37). The calculated Pt- and Pd−DFO−B stability constants are larger than those for most divalent cations, but smaller than a majority of those for the trivalent cations, including Fe(III) (Table 3). Therefore, based on our experimental results in a natural environment and assuming the behavior of DFO−B to be similar to other natural siderophores, PGEs are likely to effectively compete with elements such as Ca and Mg for available siderophores, and PGE-siderophore complexes may form to a significant extent under these conditions. However, significant activities of free trivalent cations, such as Fe(III) or Al(III), are likely to limit the formation of PGE-siderophore complexes and minimize the effects of siderophores on PGE-bearing material solubilities and dissolution rates. Experiments are required to test these predictions as other factors, such as ionic activities, may play a significant role in determining relative solubility.

TABLE 3. DFO−B Metal Stability Constants (K_f) of Various Trivalent and Divalent Metal Cations[a]

trivalent	Log K_f	temp (°C)	divalent	Log K_f	temp (°C)
Fe	30.7	25	Sn	21.14	25
Ga	28.17	25	Pd	19.2−23.2	25
Al	24.14	25	Pt	16.2−17.2	25
In	20.6	25	Cu	14.12	20
Bi	∼23.5[a]	25	Ni	10.9	20
Yb	16	20	Co	10.31	20
La	10.89	20	Zn	10.07	20
			Pb	10[a]	25
			Cd	7.88	20
			Mg	4.3	20
			Ca	2.64	20
			Sr	2.2	20

All values reported at ionic strength of 0.1. [a]Data from ref *13* with the following exceptions: Sn is from ref *12* and Pd and Pt are determined in this study and adjusted to 0.1 M, for comparison, with the extended Debye−Hückel formula.

Although competition between the PGEs and other metals found in soils, especially Fe(III), for the DFO−B complexation sites was not directly considered in this study, our results clearly demonstrate that, under certain environmentally relevant circumstances, siderophores could significantly increase the solubility of PGEs at pH 7 in the order of Pd > Pt > Rh. DFO−B appears to have little to no influence on the dissolution of Rh and Rh_2O_3. As catalytic converter-emitted PGEs are primarily in the metallic form upon release to the roadside (*1*), the metallic Pd and Pt results are the most pertinent to predict how siderophores might influence dissolution of such particles. Although less soluble than their oxide forms, zerovalent Pd and Pt metals are still affected by the presence of DFO−B, as shown in Figures 1 and 2. This work adds to growing evidence that the PGEs may be more mobile than originally believed (see ref *1*), which has implications for bioavailablity of these metals in the environment. Based on the positive results presented here, further work is underway to address the behavior of catalytic converter material to account for the nanocrystalline structure of the PGEs in the wash coat and competition of other metals found in the catalytic converters.

Acknowledgments

This material is based on work supported under a National Science Foundation Graduate Research Fellowship to S.R.D. and through a NSF Environmental Molecular Science Institute grant (EAR02-21966) to University of Notre Dame, and EAR 03-21161 to C.R.N. This paper greatly benefited from discussion with Scott Wood and from three anonymous reviewers.

Supporting Information Available

Additional information discussing the detailed sample preparation and analyses methods and consideration of DFO−B breakdown. This material is available free of charge via the Internet at http://pubs.acs.org.

Literature Cited

(1) Ek, K. H.; Morrison, G. M.; Rauch, S. Environmental routes for platinum group elements to biological materials—a review. *Sci. Total Environ.* **2004**, *334*−*35*, 21−38.

(2) Lustig, S.; Zang, S. L.; Beck, W.; Schramel, P. Influence of microorganisms on the dissolution of metallic platinum emitted by automobile catalytic converters. *Environ. Sci. Pollut. Res.* **1997**, *4*, 141−145.

(3) Wood, S. A. The interaction of dissolved platinum with fulvic acid and simple organic acid analogues in aqueous solutions. *Can. Miner.* **1990**, *28*, 665−673.
(4) Wood, S. A.; Tait, C. D.; Vlassopoulos, D.; Janecky, D. R. Solubility and spectroscopic studies of the interaction of palladium with simple carboxylic-acids and fulvic-acid at low-temperature. *Geochim. Cosmochim. Acta* **1994**, *58*, 625−637.
(5) Bowles, J. F. W.; Gize, A. P. A preliminary study of the release of platinum and palladium from metallic particles in the surface environment by organic acids: relevance to weathering of particles from vehicle exhaust catalysts. *Mineral. Mag.* **2005**, *69*, 687−693.
(6) Lustig, S.; Zang, S. L.; Beck, W.; Schramel, P. Dissolution of metallic platinum as water soluble species by naturally occurring complexing agents. *Mikrochim. Acta* **1998**, *129*, 189−194.
(7) Kraemer, S. M. Iron oxide dissolution and solubility in the presence of siderophores. *Aquat. Sci.* **2004**, *66*, 3−18.
(8) Ams, D. A.; Maurice, P. A.; Hersman, L. E.; Forsythe, J. H. Siderophore production by an aerobic *Pseudomonas mendocina* bacterium in the presence of kaolinite. *Chem. Geol.* **2002**, *188*, 161−170.
(9) Moldovan, M.; Palacios, M. A.; Gomez, M. M.; Morrison, G.; Rauch, S.; McLeod, C.; Ma, R.; Caroli, S.; Alimonti, A.; Petrucci, F.; Bocca, B.; Schramel, P.; Zischka, M.; Pettersson, C.; Wass, U.; Luna, M.; Saenz, J. C.; Santamaria, J. Environmental risk of particulate and soluble platinum group elements released from gasoline and diesel engine catalytic converters. *Sci. Total Environ.* **2002**, *296*, 199−208.
(10) Oakes, A. J.; Vickerman, J. C. SIMS investigation of fresh and aged automotive exhaust catalysts. *Surf. Interface Anal.* **1996**, *24*, 695−703.
(11) Frazier, S. W.; Kretzschmar, R.; Kraemer, S. M. Bacterial siderophores promote dissolution of UO_2 under reducing conditions. *Environ. Sci. Technol.* **2005**, *39*, 5709−5715.
(12) Hernlem, B. J.; Vane, L. M.; Sayles, G. D. Stability constants for complexes of the siderophore desferrioxamine B with selected heavy metal cations. *Inorg. Chim. Acta* **1996**, *244*, 179−184.
(13) Martell, A. E.; Smith, R. E. *NIST Stability Constants of Metal Complexes Database 46*, 6.0; U.S. Department of Commerce: Gaithersburg, MD, 2001.
(14) Renshaw, J. C.; Robson, G. D.; Trinci, A. P. J.; Wiebe, M. G.; Livens, F. R.; Collison, D.; Taylor, R. J. Fungal siderophores: structures, functions and applications. *Mycol. Res.* **2002**, *106*, 1123−1142.
(15) Enyedy, E. A.; Pocsi, I.; Farkas, E. Complexation and divalent of desferricoprogen with trivalent Fe, Al, Ga, In and divalent Fe, Ni, Cu, Zn metal ions: effects of the linking chain structure on the metal binding ability of hydroxamate based siderophores. *J. Inorg. Biochem.* **2004**, *98*, 1957−1966.
(16) Hernlem, B. J.; Vane, L. M.; Sayles, G. D. The application of siderophores for metal recovery and waste remediation: Examination of correlations for prediction of metal affinities. *Water Res.* **1999**, *33*, 951−960.
(17) Normand, C.; Wood, S. A. Effect of the trihydroxamate siderophores desferrioxamine-B and ferrichrome on the mobility of Pd, Pt, Rh and Ir. *Geochim. Cosmochim. Acta* **2005**, *69*, A329−A329.
(18) Normand, C.; Wood, S. A.; Roach, L. D. Effect of the siderophore Desferrioxamine-B on the mobility of Pd. *Geochim. Cosmochim. Acta* **2004**, *68*, A359−A359.
(19) Roach, L. D.; Normand, C.; Wood, S. A. *Abstracts with Programs*, Effect of the siderophore desferrioxamine B on the mobility of palladium, September, 2003; Geological Society of America: Boulder, CO, 2003; Vol. 35, p 242.
(20) Wood, S. A. The effect of organic ligands on the mobility of the PGE in soils and natural waters: Implications for exploration and the environment. *Geochim. Cosmochim. Acta* **2005**, *69*, A329.
(21) Normand, C.; Wood, S. A. In *Pd, Pt, Rh and Ir mobility at near-neutral pH in the presence of siderophores*, 10th International Platinum Symposium, Oulu, Finland, 2005; Tormanen, T. O.; Alapieti, T. T. Eds.; International Platinum Symposium: Oulu, Finland, 2005; pp 501−504.
(22) Schlögl, R.; Indelkofer, G.; Oelhafen, P. Emission of microparticles from automotive sources—X-ray phoitoelectron spectroscopy in environmental analysis. *Chem. Int.* **1987**, *26*, 309−319.
(23) Hersman, L.; Lloyd, T.; Sposito, G. Siderophore-promoted dissolution of hematite. *Geochim. Cosmochim. Acta* **1995**, *59*, 3327−3330.
(24) Hepinstall, S. E.; Turner, B. F.; Maurice, P. A. Effects of siderophores on Pb and Cd adsorption to kaolinite. *Clays Clay Miner.* **2005**, *53*, 557−563.
(25) Kraemer, S. M.; Xu, J. D.; Raymond, K. N.; Sposito, G. Adsorption of Pb(II) and Eu(III) by oxide minerals in the presence of natural and synthetic hydroxamate siderophores. *Environ. Sci. Technol.* **2002**, *36*, 1287−1291.
(26) Rosenberg, D. R.; Maurice, P. A. Siderophore adsorption to and dissolution of kaolinite at pH 3 to 7 and 22 degrees C. *Geochim. Cosmochim. Acta* **2003**, *67*, 223−229.
(27) Kraemer, S. M.; Hering, J. G. Influence of solution saturation state on the kinetics of ligand-controlled dissolution of oxide phases. *Geochim. Cosmochim. Acta* **1997**, *61*, 2855−2866.
(28) Kraemer, S. M.; Cheah, S. F.; Zapf, R.; Xu, J. D.; Raymond, K. N.; Sposito, G. Effect of hydroxamate siderophores on Fe release and Pb(II) adsorption by goethite. *Geochim. Cosmochim. Acta* **1999**, *63*, 3003−3008.
(29) Mountain, B. W.; Wood, S. A. Chemical controls on the solubility, transport, and deposition of platinum and palladium in hydrothermal solutions—a thermodynamic approach. *Econ. Geol.* **1988**, *83*, 492−510.
(30) Wood, S. A.; Mountain, B. W.; Fenlon, B. J. Thermodynamic constraints on the solubility of platinum and palladium in hydrothermal solutions—reassessment of hydroxide, bisulfide, and ammonia complexing. *Econ. Geol.* **1989**, *84*, 2020−2028.
(31) Fein, J. Experimental study of aluminum-, calcium-, and magnesium-acetate complexing at 80 °C. *Geochim. Cosmochim. Acta* **1991**, *55*, 955−964.
(32) Helgeson, H. C.; Kirkham, D. H.; Flowers, G. C. Theoretical prediction of the thermodynamic behavior of aqueous-electrolytes at high-pressures and temperatures.4. Calculation of activity-coefficients, osmotic coefficients, and apparent molal and standard and relative partial molal properties to 600-degrees-C and 5 Kb. *Am. J. Sci.* **1981**, *281*, 1249−1516.
(33) Azaroual, M.; Romand, B.; Freyssinet, P.; Disnar, J. R. Solubility of platinum in aqueous solutions at 25 degrees C and pHs 4 to 10 under oxidizing conditions. *Geochim. Cosmochim. Acta* **2001**, *65*, 4453−4466.
(34) Byrne, R. H. Comment on "Solubility of platinum in aqueous solutions at 25 degrees C and pHs 4 to 10 under oxidizing conditions" by Mohamed Azaroual, Bruno Romahd, Philippe Freyssinet, and Jean-Robert Disnar. *Geochim. Cosmochim. Acta* **2003**, *67*, 2509−2509.
(35) van Middlesworth, J. M.; Wood, S. A. The stability of palladium(II) hydroxide and hydroxy-chloride complexes: An experimental solubility study at 25−85. degrees C and 1 bar. *Geochim. Cosmochim. Acta* **1999**, *63*, 1751−1765.
(36) Sassani, D. C.; Shock, E. L. Solubility and transport of platinum-group elements in supercritical fluids: Summary and estimates of thermodynamic properties for ruthenium, rhodium, palladium, and platinum solids, aqueous ions, and complexes to 1000 degrees C and 5 kbar. *Geochim. Cosmochim. Acta* **1998**, *62*, 2643−2671.
(37) Wood, S. A.; Mountain, B. W.; Pan, P. The aqueous geochemistry of platinum, palladium and gold—recent experimental constraints and a reevaluation of theoretical predictions. *Can. Mineral* **1992**, *30*, 955−982.
(38) Ely, J. C.; Neal, C. R. Method of data reduction and uncertainty estimation for platinum-group element data using inductively coupled plasma-mass spectrometry. *Geostand. Newsl.* **2002**, *26*, 31−39.
(39) Brookins D. G. *Eh-pH Diagrams for Geochemistry*; Springer-Verlag: New York, 1988.

Received for review June 19, 2006. Revised manuscript received October 17, 2006. Accepted October 25, 2006.

ES0614666